Control of Energy Density inside a Disordered Medium by Coupling to Open or Closed Channels

Raktim Sarma,[1] Alexey G. Yamilov,[2,*] Sasha Petrenko,[2] Yaron Bromberg,[1] and Hui Cao[1,†]
[1]Department of Applied Physics, Yale University, New Haven, Connecticut 06520, USA
[2]Department of Physics, Missouri University of Science & Technology, Rolla, Missouri 65409, USA
(Received 6 June 2016; published 17 August 2016)

We demonstrate experimentally the efficient control of light intensity distribution inside a random scattering system. The adaptive wave front shaping technique is applied to a silicon waveguide containing scattering nanostructures, and the on-chip coupling scheme enables access to all input spatial modes. By selectively coupling the incident light to the open or closed channels of the disordered system, we not only vary the total energy stored inside the system by a factor of 7.4, but also change the energy density distribution from an exponential decay to a linear decay and to a profile peaked near the center. This work provides an on-chip platform for controlling light-matter interactions in turbid media.

DOI: 10.1103/PhysRevLett.117.086803

It has long been known that in disordered media there are many fascinating and surprising effects resulting from the interferences of multiply scattered waves [1,2]. One of them is the creation of transmission eigenchannels, which can be broadly classified as either open or closed [3,4]. The existence of high-transmission (open) channels allows for an optimally prepared coherent input beam to be transmitted through a lossless diffusive medium with order unity efficiency. In contrast, waves injected into low-transmission (closed) channels barely penetrate the medium and are mostly reflected. In general, the penetration depth and energy density distribution of multiply scattered waves inside a disordered medium are determined by the spatial profiles of the transmission eigenchannels that are excited by the incident light. The distinct spatial profiles of the open and closed channels suggest that selective coupling of incident light to these channels enables the effective control of the total transmission and energy distribution inside the random medium [5,6]. Since the energy density determines the light-matter interactions inside a scattering system, manipulating its spatial distribution opens the door to tailoring optical excitations as well as linear and nonlinear optical processes such as absorption, emission, amplification, and frequency mixing inside turbid media. The potential applications range from photovoltaics [7,8], white light emitting diodes [9], and random lasers [10], to biomedical sensing [11] and radiation treatments [12].

In recent years there have been numerous theoretical and experimental studies on transmission eigenchannels [5,13–17]. While by knowing the transmission matrix one can determine their profiles [18–21], it is difficult to directly probe their spatial profiles inside three-dimensional (3D) random media. So far, open and closed channels have been observed only with an acoustic wave inside a two-dimensional (2D) disordered waveguide [22], but controlling the energy density distribution has not been realized due to the lack of an efficient wave front modulator for acoustic wave or microwave radiation. The advantage of optical waves is the availability of spatial light modulators (SLMs) with many degrees of freedom. However, the commonly used samples in an optical experiment have an open slab geometry, thus making it impossible to control all input modes due to the limited numerical aperture of the imaging optics. Such incomplete control dramatically weakens the open channels [23], although a notable enhancement of the total transmission has been achieved [20,24]. Furthermore, an enhancement of the total energy stored inside a 3D scattering sample has been reported [25], but a direct probe and control of the optical intensity distribution inside the scattering medium are still missing.

In this Letter, we demonstrate experimentally the control of the energy density distribution inside a scattering medium. Instead of the open slab geometry, we fabricate a silicon waveguide that contains scatterers and has reflecting sidewalls. The intensity distribution inside the two-dimensional waveguide is probed from the third dimension. With careful design of the on-chip coupling waveguide, we can access all the input modes. Such control of the incident wave front enables an order of magnitude enhancement of the total transmission or a 50 times suppression. A direct probe of the optical intensity distribution inside the disordered waveguide reveals that the selective excitation of the open channels results in the buildup of energy deep inside the scattering medium, while the excitation of the closed channels greatly reduces the penetration depth. Compared to the linear decay for random input fields, the optimized wave front can produce an intensity profile that either is peaked near the center of the waveguide or decays exponentially with depth. The total energy stored inside the waveguide is increased 3.7 times or decreased 2 times.

The 2D waveguide structure was fabricated in a 220 nm silicon layer on top of a 3 μm buried oxide by electron

beam lithography and reactive ion etching [6]. As shown in Fig. 1, air holes are randomly distributed within the waveguide whose sidewalls are a photonic crystal that reflects light. At the probe wavelength $\lambda = 1.51$ μm, the transport mean free path $\ell = 2.5$ μm is much less than the length $L = 50$ μm of the disordered waveguide, so that the light transport is diffusive. The out-of-plane scattering, which provides a direct probe of the light transport inside the random structure, can be treated as loss and the diffusive dissipation length is $\xi_a = 31$ μm. The values of ℓ and ξ_a were extracted from the measured intensity distribution and intensity fluctuations inside the disordered waveguide for uncontrolled illumination [26]. The waveguide of width $W = 15$ μm supports $N = 56$ transmission eigenchannels, among which ~5 are open channels and the rest are closed channels. The total transmission for the uncontrolled illumination is about 4.8%.

The probe light is injected into the waveguide from the edge of the wafer. Because of the large mismatch of the refractive index between silicon and air, the light can be coupled only to the lower-order modes of the ridge waveguide. This limits the number of input modes that can be controlled by wave front shaping. To increase the degree of input control, the coupling waveguide (lead) is tapered at an angle of 15° [Fig. 1(a)]. The wider waveguide at the front end supports many more lower-order modes, which can be excited by the incident light and then converted to high-order modes by the taper [27]. As detailed in the Supplemental Material [27], we set $W_1 = 330$ μm for the fabricated sample in Fig. 1, so that the number of waveguide modes excited at the air-silicon interface is significantly larger than N. This ensures all input modes to the disordered waveguide are accessed by the incident fields with phase-only modulation.

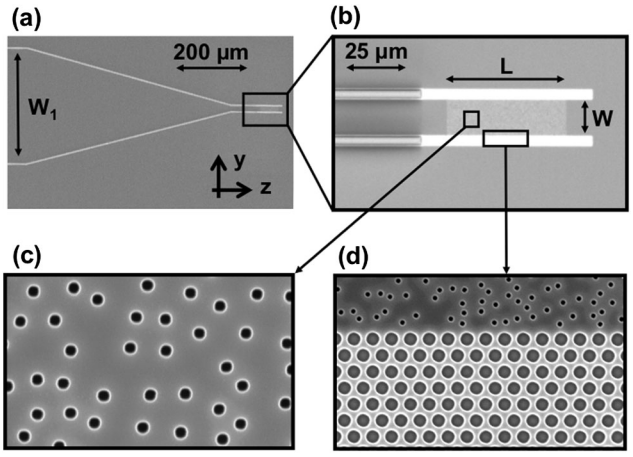

FIG. 1. On-chip disordered waveguide with a tapered lead. (a) Top-view scanning electron micrograph (SEM) of a fabricated silicon waveguide. A ridge waveguide (lead) is tapered from the width $W_1 = 330$ μm at the edge of the wafer to the width $W = 15$ μm, in order to increase the degree of control of the light that is injected to the disordered waveguide. (b) Magnified SEM of the disordered region of the waveguide that consists of a random array of air holes (diameter = 90 nm). (c) Magnified SEM showing the air holes distributed randomly within the waveguide with a filling fraction of 6%. (d) The sidewalls of the waveguide are made of a triangular lattice of air holes (diameter = 360 nm) with a lattice constant of 505 nm, which supports a full photonic band gap at the wavelength $\lambda = 1.51$ μm.

The wave front shaping experiment is shown schematically in Fig. 2(a) and detailed in the Supplemental Material [27]. A monochromatic laser beam is phase modulated by a SLM and then focused to the edge of the wafer by a microscope objective of numerical aperture (NA) 0.7. To produce a line of illumination at the input facet of the coupling waveguide, the SLM imposes phase modulation only along one dimension that is parallel to the transverse direction of the waveguide, as shown by the 2D phase mask in Fig. 2(a). The light that is scattered out of plane by the random array of air holes is collected by an objective and projected to an InGaAs camera to obtain the spatial

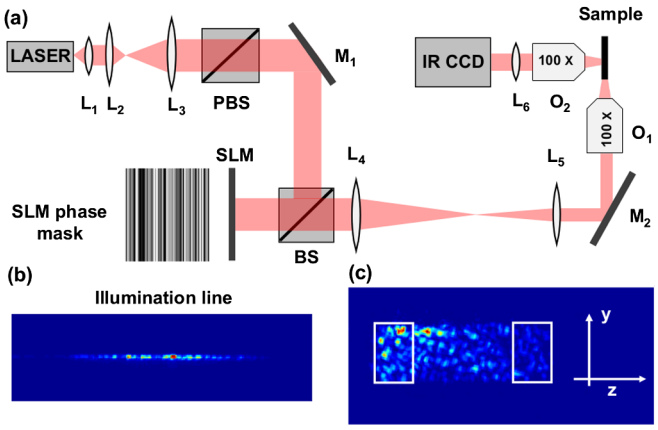

FIG. 2. Wave front shaping experiment to control the intensity distribution inside a disordered waveguide. (a) A schematic of the experimental setup. Laser (HP 8168F) output at $\lambda = 1510$ nm is collimated (by lens L_1), expanded (by L_2, L_3), and linearly polarized (by a polarized beam splitter PBS) before being modulated by a phase-only SLM (Hamamatsu X10468). Two lenses (L_4, L_5) are used to project the SLM plane to the pupil plane of an objective O_1 (100×, NA = 0.7), and the edge of the wafer is placed at the focal plane. The SLM imposes phase modulation only in one direction in order to generate a line at the front end of the coupling waveguide. A sample phase pattern on the SLM is shown. The light scattered out of the sample plane is collected by another objective O_2 (100×, NA = 0.7) and imaged to an InGaAs camera (Xenics XEVA 1.7-320) by a tube lens (L_6). M_1 and M_2 are mirrors and BS is a beam splitter. (b) An optical image of the illumination line (330 × 1.1 μm) on the waveguide facet. The input intensity is modulated along the line. (c) An image of the spatial distribution of the light intensity inside the disordered waveguide for a random input wave front. The spatial resolution is about 1.1 μm. The ratio S of the integrated intensities over the two rectangles at the back and front side of the waveguide is used as feedback for optimizing the input wave front.

distribution of the intensity $I(y,z)$ inside the disordered structure [Fig. 2(c)].

Two wave front shaping approaches have been developed for the transmission enhancement: one is based on the measurement of the transmission matrix [28,29]; the other relies on feedback [30]. While the open channels can be obtained from the measured transmission matrix, the closed channels are subject to measurement noise due to the nearly vanishing transmission. Here, we took the feedback approach, and optimized the procedure using the continuous sequential algorithm [30] to control the energy density inside the disordered waveguide. The cost function S is the ratio of the light intensity integrated over an area in the back part of the waveguide to that in the front part [marked by two rectangles in Fig. 2(c)].

First, we maximize S to enhance the light penetration into the scattering structure. Figure 3(b) shows the final intensity distribution $I(y,z)$ for the optimized input. In Fig. 3(e) we plot the cross-section-averaged intensity $I(z) = \int_0^W I(y,z)dy$, further averaged over four wavelengths and three initial phase patterns that served as the seed to the optimization algorithm [27]. $I(z)$ is peaked near the center of the disordered waveguide in Fig. 3(e), which is dramatically different from the monotonic decay with random input fields in Fig. 3(d). The latter profile is in agreement with the prediction of diffusion theory and the slight deviation from a linear decay is caused by the out-of-plane scattering loss. The dissipation causes an asymmetry in the optimized intensity distribution with respect to the center of the waveguide ($z/L = 0.5$), as the peak of $I(z)$ in Fig. 3(b) shifts towards the input end. Such an asymmetry is captured by the maximum transmission channel, but not by the fundamental diffusion mode [25] or the return probability [5]. The resemblance of the optimized $I(z)$ to the spatial profile of the open channels indicates that the optimized wave front couples light to the high-transmission eigenchannels.

Next, we minimize S by adapting the input wave front, and the resulting intensity distribution is presented in Fig. 3(c). The cross-section-averaged intensity $I(z)$ in Fig. 3(f) exhibits a much faster decay with depth than the random input. Moreover, the decay is clearly exponential, resembling the spatial profile of the closed channels. Despite the presence of measurement noise, the optimized wave front couples effectively to the low-transmission eigenchannels.

To confirm the experimental results, we simulate a 2D disordered waveguide with all parameters equal to the experimental values [27,31]. The phase-only modulation is imposed on the input wave front to optimize the same cost function S with the continuous sequential algorithm (details in the Supplemental Material) [27]. The solid curves in Figs. 3(d)–3(f) represent the simulation results, which agree well with the experimental data. The curves are normalized such that the total incoming flux is equal to unity in all cases. Therefore, the intensity profiles can be quantitatively compared to get the order of magnitude of the intensity amplification within the scattering sample.

By projecting the optimized fields onto the transmission eigenchannels, we obtain the contributions from the individual channels. Figure 4(a) presents the weight w of each channel as a function of the transmission eigenvalue τ in the case that the cost function S is maximized [Figs. 3(b) and 3(e)]. In comparison to a random input field, which has equal contributions from all channels, $w(\tau) = 1/N$, the optimized field for maximum S has greatly enhanced contributions from the high transmission channels and reduced contributions from the low-transmission channels [Fig. 4(a)]. While the maximum transmission channel has the largest weight, a few channels with slightly lower transmission also make significant contributions. Thus, the energy density distribution $I(z)$ is slightly lower than that of the maximum transmission channel, and shifted a bit towards the front end of the waveguide [Fig. 4(b)]. As shown in Fig. 4(a), the weight $w(\tau)$ increases exponentially with τ, in contrast to the linear increase of w with τ in the case of focusing (maximizing intensity of a single speckle) through a random medium. This difference indicates

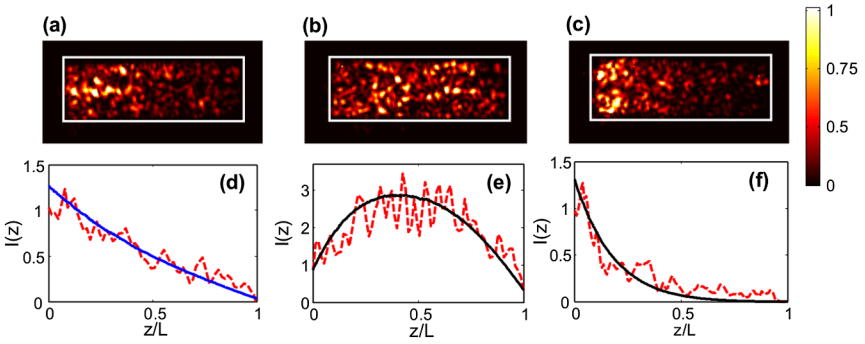

FIG. 3. Experimental control of the intensity distribution inside the disordered waveguide. (a)–(c) Two-dimensional intensity distribution $I(y,z)$ inside the disordered waveguide shown in Fig. 1 for (a) random input fields, (b) optimized input for maximum light penetration (maximizing S), and (c) optimized input for minimum light penetration (minimizing S). (d)–(f) The cross-section-averaged intensity $I(z)$ obtained from $I(y,z)$ in (a)–(c). The dashed lines are experimental data and the solid lines are simulation results.

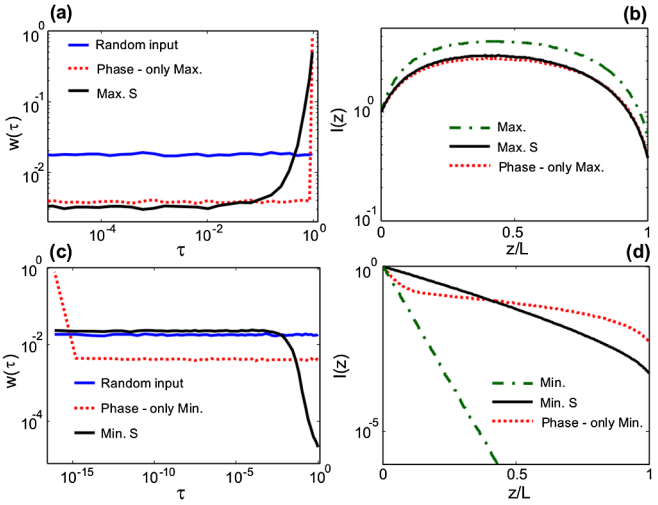

FIG. 4. Numerical simulation of the wave front shaping experiment. (a),(c) Weight $w(\tau)$ of each transmission eigenchannel in the input field obtained by maximizing (a) or minimizing (c) the light penetration into the disordered waveguide with the cost function S (black solid line). For comparison, $w(\tau)$ for the random input field (blue solid line) and for the input field of the maximum (a) or minimum (c) transmission eigenchannel after removal of amplitude modulation (red dotted line) are also shown. (b),(d) Cross-section-averaged intensity distribution $I(z)$ for the maximized (b) or minimized (d) S (black solid line), as well as the maximum (b) or minimum (d) transmission channel with (green dash-dotted line) and without amplitude modulation (red dotted line).

maximizing S is more efficient for enhancing the contribution of the maximum transmission channel over all other channels.

When S is minimized [Figs. 3(c) and 3(f)], the weights of the high-transmission channels are strongly suppressed, especially the highest transmission channel [Fig. 4(c)]. While many low-transmission channels have slightly increased weights as compared to the random input field, none of them becomes dominant. Since the low-transmission channels have exponential decay with different decay lengths, the total intensity distribution $I(z)$ obtained by minimizing S also decays exponentially, but the decay length is longer than that of the minimum transmission channel [Fig. 4(d)].

The numerical simulation confirms that our wave front shaping experiment results in selective coupling of the input light to open or closed channels, which leads to a distinct intensity distribution inside the scattering waveguide. The total transmission is increased from ~4.8% (for random input fields) to ~47% (when S is maximized), and the total energy inside the disordered structure is enhanced 3.7 times. The minimization of S makes the total transmission drop to ~0.1%, and the total energy inside is reduced by a factor of 2.

Finally, we compare numerically the feedback-based approach to the transmission-matrix approach by computing the transmission eigenchannels from the field transmission matrix. With phase-only modulation, the input field for a transmission eigenchannel is decomposed by the waveguide modes, and the amplitudes of the decomposition coefficients are set to a constant. The removal of amplitude modulation mixes the maximum transmission channel with other channels, as seen in Fig. 4(a). While the weight of the maximum transmission channel decreases from unity to $\pi/4$ [32], all other channels have a constant weight $[1-(\pi/4)]/(N-1)$. The cross-section-averaged intensity distribution $I(z)$ is nearly identical to that obtained by maximizing S [Fig. 4(b)]. Similarly, the elimination of amplitude modulation from the minimum transmission channel introduces contributions from all other channels [Fig. 4(c)]. Their weights are equal (independent of their transmission), albeit smaller than that of the minimum transmission channel. Consequently, $I(z)$ displays a rapid decay at shallow depths, due to the dominant contribution from the minimum transmission channel; it is followed by a much slower decay at large depth due to the contributions of the remaining channels including the highly transmitting ones. The total transmission is ~1%, approximately an order of magnitude higher than that obtained by minimizing S. This is attributed to the stronger suppression of the higher transmission channels by the feedback approach, i.e., the higher the transmission eigenvalue is, the lower the weight. Therefore, with phase-only modulation of the incident wave front, the feedback approach is far more efficient in minimizing the total transmission than the transmission-matrix approach.

In summary, we apply the adaptive wave front shaping technique to on-chip disordered nanostructures. Careful design of the coupling waveguide enables access to all input modes and allows us to reach the maximum or minimum transmission that is achievable with phase-only modulation. Selective excitation of the open or closed channels results in the variation of the optical intensity distribution from an exponential decay to a linear decay and to a profile peaked near the center of the random system. The coherent control of multiple-scattering interference leads to diverse transport behaviors in contrast to universal diffusion, highlighting the possibility of controlling light-matter interactions in turbid media.

We acknowledge Chia-Wei Hsu, Douglas Stone, Hasan Yilmaz, Seng Fatt Liew, and Brandon Redding for useful discussions. This work was supported by the National Science Foundation under Grants No. DMR-1205307 and No. DMR-1205223. Facilities use was supported by YINQE and NSF MRSEC Grant No. DMR-1119826.

*yamilov@mst.edu
†hui.cao@yale.edu

[1] M. C. W. van Rossum and T. M. Nieuwenhuizen, Rev. Mod. Phys. **71**, 313 (1999).

[2] E. Akkermans and G. Montambaux, *Mesoscopic Physics of Electrons and Photons* (Cambridge University Press, Cambridge, England, 2007).
[3] O. N. Dorokhov, Solid State Commun. **51**, 381 (1984).
[4] Y. Imry, Europhys. Lett. **1**, 249 (1986).
[5] M. Davy, Z. Shi, J. Park, C. Tian, and A. Z. Genack, Nat. Commun. **6**, 6893 (2015).
[6] R. Sarma, A. Yamilov, S. F. Liew, M. Guy, and H. Cao, Phys. Rev. B **92**, 214206 (2015).
[7] K. Vynck, M. Burresi, F. Riboli, and D. S. Wiersma, Nat. Mater. **11**, 1017 (2012).
[8] D. S. Wiersma, Nat. Photonics **7**, 188 (2013).
[9] V. Y. F. Leung, A. Lagendijk, T. W. Tukker, A. P. Mosk, W. L. Ijzerman, and W. L. Vos, Opt. Express **22**, 8190 (2014).
[10] X. Cheng and A. Z. Genack, Opt. Lett. **39**, 6324 (2014).
[11] Q. Song, S. Xiao, Z. Xu, V. M. Shalaev, and Y. L. Kim, Opt. Lett. **35**, 2624 (2010).
[12] J. Yoon, M. Lee, K. Lee, N. Kim, J. M. Kim, J. Park, H. Yu, C. Choi, W. Do Heo, and Y. Park, Sci. Rep. **5**, 13289 (2015).
[13] I. M. Vellekoop and A. P. Mosk, Phys. Rev. Lett. **101**, 120601 (2008).
[14] A. P. Mosk, A. Lagendijk, G. Lerosey, and M. Fink, Nat. Photonics **6**, 283 (2012).
[15] W. Choi, A. P. Mosk, Q. Han Park, and W. Choi, Phys. Rev. B **83**, 134207 (2011).
[16] A. Peña, A. Girschik, F. Libisch, S. Rotter, and A. A. Chabanov, Nat. Commun. **5**, 3488 (2014).
[17] S. F. Liew, S. M. Popoff, A. P. Mosk, W. L. Vos, and H. Cao, Phys. Rev. B **89**, 224202 (2014).
[18] S. M. Popoff, G. Lerosey, R. Carminati, M. Fink, A. C. Boccara, and S. Gigan, Phys. Rev. Lett. **104**, 100601 (2010).
[19] Z. Shi and A. Z. Genack, Phys. Rev. Lett. **108**, 043901 (2012).
[20] M. Kim, Y. Choi, C. Yoon, W. Choi, J. Kim, Q. H. Park, and W. Choi, Nat. Photonics **6**, 581 (2012).
[21] H. Yu, T. R. Hillman, W. Choi, J. O. Lee, M. S. Feld, R. R. Dasari, and Y. K. Park, Phys. Rev. Lett. **111**, 153902 (2013).
[22] B. Gerardin, J. Laurent, A. Derode, C. Prada, and A. Aubry, Phys. Rev. Lett. **113**, 173901 (2014).
[23] A. Goetschy and A. D. Stone, Phys. Rev. Lett. **111**, 063901 (2013).
[24] S. M. Popoff, A. Goetschy, S. F. Liew, A. D. Stone, and H. Cao, Phys. Rev. Lett. **112**, 133903 (2014).
[25] O. S. Ojambati, H. Yilmaz, A. Lagendijk, A. P. Mosk, and W. L. Vos, New J. Phys. **18**, 043032 (2016).
[26] R. Sarma, A. Yamilov, P. Neupane, and H. Cao, Phys. Rev. B **92**, 180203 (2015).
[27] See Supplemental Material at http://link.aps.org/supplemental/10.1103/PhysRevLett.117.086803 for detail description about the experimental setup, structure design and numerical simulations.
[28] M. Kim, W. Choi, Y. Choi, C. Yoon, and W. Choi, Opt. Express **23**, 12648 (2015).
[29] H. Yu, J. Park, K. Lee, J. Yoon, K. Kim, S. Lee, and Y. Park, Curr. Appl. Phys. **15**, 632 (2015).
[30] I. M. Vellekoop, Opt. Express **23**, 12189 (2015).
[31] C. W. Groth, M. Wimmer, A. R. Akhmerov, and X. Waintal, New J. Phys. **16**, 063065 (2014).
[32] I. M. Vellekoop, E. G. Van Putten, A. Lagendijk, and A. P. Mosk, Opt. Express **16**, 67 (2008).

Control of energy density inside disordered medium by coupling to open or closed channels

Raktim Sarma,[1] Alexey G. Yamilov,[2,*] Sasha Petrenko,[2] Yaron Bromberg,[1] and Hui Cao[1,†]

[1]*Department of Applied Physics, Yale University, New Haven, CT, 06520, USA*
[2]*Department of Physics, Missouri University of Science & Technology, Rolla, Missouri 65409, USA*

(Dated: July 27, 2016)

PACS numbers: 42.25.Bs, 42.25.Dd, 73.23.-b

I. DESIGN OF COUPLING WAVEGUIDE

To select the parameters for the tapered lead, we compute the degree of control for the optical field at the end of the lead that will be injected to the disordered waveguide. We simulate light propagation through the tapered waveguide using the Finite Element Method (COMSOL) and KWANT [1]. At the entrance of the lead ($z = 0$), only low-order modes (up to $M_1 - th$ order) of the waveguide (of width W_1) are excited with constant amplitude and random phase. The incident electric field can be written as

$$E(y, z = 0) = \sum_{m=1}^{M_1} e^{i\theta_m} \phi_m(y),$$

where $\phi_m(y)$ represents the transverse field profile for the $m - th$ guided mode, and θ_m is the initial phase. We calculate electric field distribution at the end of the lead $E_n(y, z = L_1)$, where the subscript n denotes different set of random phases θ_m assigned to the input field, L_1 is the length of the tapered lead. Then we construct the covariance matrix,

$$C(y, y') = \langle E_n(y) E_n^*(y') \rangle_n,$$

where $\langle\rangle_n$ represents averaging over random input wavefields. The eigenvalues of $C(y, y')$ are computed and plotted in Fig. S1 for a tapered waveguide of $W_1 = 85$ μm, $W = 15$ μm, and $L_1 = 100$ μm. The sudden drop of the eigenvalues in Fig. S1 gives the number of significant eigenvalues, which corresponds to the number of independent spatial modes M that are controlled by varying the input field [Fig. S1]. We compute M for many tapered waveguides of different dimensions, and find $M = N$ as long as M_1 exceeds the number of transverse modes N at the end of the lead (of width W).

In the experiment, the number of low-order modes in the coupling waveguide that are excited by the incident light, M_1, depends on the numerical aperture (NA) of the objective we used to couple light into the silicon waveguide, the refractive index contrast at the silicon/air interface, the width W_1 and NA of the silicon waveguide. For the fabricated sample in Fig. 1, $W_1 = 330$ μm, the total number of waveguide modes at the front of the taper is 1245. The numerical aperture of the objective (NA = 0.7) determines the range of incident angle for light illuminating the front facet of the silicon waveguide. From the silicon/air index contrast, we calculate the angular range of light that is coupled into the waveguide, and then obtain the number of waveguide modes that are excited by the incident light, $M_1 = 359$. We intentionally made M_1 much larger than $N = 56$, to ensure all input modes to the disordered waveguide are accessed experimentally. In addition, we adjust the incident beam size to completely fill the pupil of the objective, so that the entire numerical aperture of the objective is used to couple light into the lead.

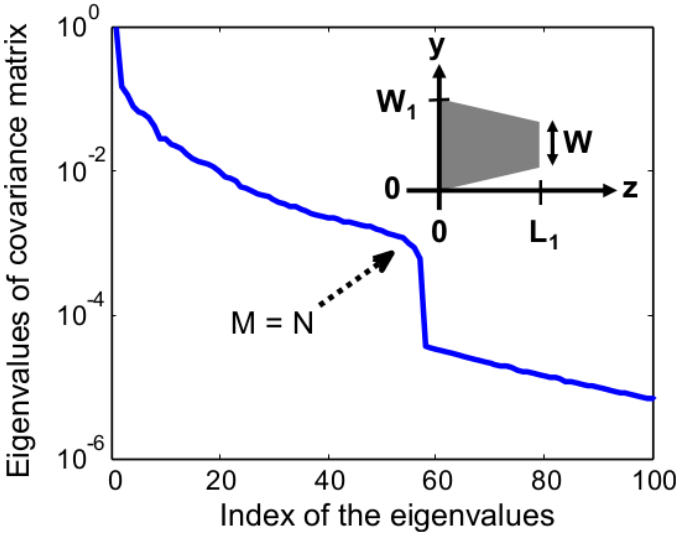

FIG. S1: Semi-log plot of the eigenvalues of the covariance matrix $C(y, y')$ for the electric field $E_m(y, z = L_1)$ at the end of a tapered lead with $W_1 = 85$ μm, $W = 15$ μm, and $L_1 = 100$ μm. The inset is a schematic of the geometry. The sudden drop of eigenvalues gives the number of significant eigenvalues, $M = 56$, which is equal to the number of waveguide modes $N = 56$ at the end of the lead $z = L_1$.

II. WAVEFRONT SHAPING EXPERIMENT

In the wavefront shaping experiment, we modulate the phases of 300 macro-pixels on the SLM. Each macro-pixel is a group of 2×792 SLM pixels, and has the dimension 0.04×15.8 mm. Since the SLM plane is projected onto the

pupil plane of the objective (O_1), the phase modulation is applied to the phase space instead of the real space. To ensure the convergence of the optimization algorithm, the phases of all macro-pixels are adjusted in two sequential rounds. The final value of the cost function S depends on the initial phase pattern for the optimization algorithm, but the variation is less than 10%. The final distribution of light intensity across the disordered waveguide $I(y, z)$ also changes with the initial phase pattern, but the cross-section-averaged intensity $I(z)$ has almost the same profile. Thus the data obtained from different initial phase patterns are averaged to reduce fluctuations.

To optimize the throughput of the disordered waveguide, we choose the cost function to be the ratio of the cross-section integrated intensity at the back end to that at the front end. To smooth out the fluctuation, the intensity is integrated over an area of length d and width W. Experimentally we varied d from $2l$ to $7l$, where l = 2.5 μm is the transport mean free path, and the final results obtained via optimization are robust. If d is less than $2l$, the spatial averaging is not sufficient to smooth out the intensity fluctuation. The data shown in Fig. 3 are obtained with $d = 4.5l$.

To avoid experimental artifacts it is crucial to optimize the intensity ratio instead of the intensity integrated over the entire scattering sample, because the adaptive wave front shaping can change not only the energy distribution inside the sample, but also the transmission through the optical system that delivers light from the SLM to the sample. If we were to maximize or minimize the total energy within the disordered waveguide, the optimization algorithm might find a wavefront that enhances or suppresses the light delivery to the sample through the lens and the objective [2].

III. NUMERICAL SIMULATION

We consider a two-dimensional (2D) waveguide of width W. The waveguide is coupled to two leads (empty waveguides) at $z = 0$ and $z = L$, supporting $N = W/(\lambda/2)$ guided modes. Numerical simulations are based on Kwant software package [1]. It allows one to conveniently calculate the scattering matrix $\hat{S}$ of disordered waveguide defined as a collection of coupled lattice sites $|i\rangle$ in a two-dimensional (2D) grid, which is described by a tight-binding Hamiltonian

$$\hat{H}|\psi\rangle = \left[\sum_{i,j} H_{ij}|i\rangle\langle j|\right]\left(\sum_{l}\psi_l|l\rangle\right), \qquad \text{(S1)}$$

where ψ_l is the wavefunction (i.e. field) at site l (a 2D vector). We introduce disorder and absorption by adding a random on-site potential δE_{ii} and constant imaginary part $i\gamma$ to the diagonal elements as $H_{ii} = E_0 + i\gamma + \delta E_{ii}$, while keeping the nearest neighbor coupling at constant value of 1. The scattering region $0 \le z \le L$ is connected to the leads with $\delta E_{ii} = 0$ and $\gamma = 0$. This model is well suited to describe wave scattering phenomena as long as $k\ell \gg 1$. In our numerical calculations, we choose the parameters E_0, the disorder strength Δ ($-\Delta < \delta E_{ii} < \Delta$), and γ to match the experimental values of $k\ell$, L/ℓ, and L/ξ_a.

The transmission matrix $\hat{t}$ is a submatrix of $\hat{S}$, it relates the amplitudes of the propagating modes incident from the left lead ϕ_a and those of the outgoing modes in the right lead ϕ_b. Representing $\hat{t}^\dagger\hat{t} = \hat{V}\hat{\tau}\hat{V}^\dagger$ gives the diagonal matrix of eigenvalues τ_α and the corresponding eigenchannels $V_{a\alpha}$. The later can be used to project any incident field $\vec{\phi}$ onto the channels and get the weight of each eigenchannel $w_\alpha = \left|\Sigma_a V^\dagger_{\alpha a}\phi_a\right|^2$. If matrix $\hat{t}$ is known and assuming phase-only control of the incident waveguide modes, it is possible to construct $\phi_a = V_{a\alpha}/|V_{a\alpha}|$ to couple predominantly into eigenchannel α. With τ_α arranged in the decreasing order, $\alpha = 1, N$ correspond to the maximum, minimum transmission eigenchannels. Selective coupling to such channel offers an opportunity to maximize or minimize the total transmission through the random system.

Alternatively, the total transmission can be maximized/minimized via continuous sequential phase optimization of the incident fields in the form $\phi_a = \exp[i\delta_a]$, where phase angles δ_a are to be determined iteratively. To compare the experimental results shown in Fig. 3 (d, e, f), such an continuous sequential phase optimization algorithm was used in the numerical calculation.

To find the intensity profile throughout the disordered region, the incident vector ϕ_a is propagated for different z and the resulting intensity $|\psi_l|^2$ is averaged over the cross section of the waveguide. In all our simulations we also performed statistical averages over 10^3 configurations of disordered potential δE_{ii}. In addition, we investigated the effects due to the tapered lead (see Fig. 1 (a) in the main text) and index mismatch between the taper and the outside region, i.e. air in our experiment. The difference in the intensity profiles shown in Figs. 3, 4 is negligible as long as the number of modes that can be excited at the front end of the tapered lead well exceeds the number of transverse modes inside the disordered waveguide.

Lastly, once we know w_α and τ_α and confirm that numerically calculated intensity profiles match the experimentally measured ones $I(z)$ in Fig. 3 (d, e, f) , we compute the total transmission, $\sum_{\alpha=1}^{N} w_\alpha\tau_\alpha$, and the total energy stored inside the disordered waveguide.

* Electronic address: yamilov@mst.edu
† Electronic address: hui.cao@yale.edu

[1] C. W. Groth, M. Wimmer, A. R. Akhmerov, and X. Waintal, *New Jour. of Phys.* **16**, 063065 (2014).

[2] S. M. Popoff, A. Goetschy, S. F. Liew, A. D. Stone, and H. Cao, *Phys. Rev. Lett.* **112**, 133903 (2014).